ORIGINAL RESEARCH

Loss of ANT1 Increases Fibrosis and Epithelial Cell Senescence in Idiopathic Pulmonary Fibrosis

Justin Sui*, Jennifer C. Boatz*, Jian Shi, Qianjiang Hu, Xiaoyun Li, Yingze Zhang, Melanie Königshoff, and Corrine R. Kliment

Pulmonary Allergy and Critical Care Medicine, Department of Medicine, University of Pittsburgh, Pittsburgh, Pennsylvania

ORCID IDs: 0000-0001-9414-5128 (M.K.); 0000-0002-3815-9370 (C.R.K.).

Abstract

Idiopathic pulmonary fibrosis (IPF) is an interstitial lung disease characterized by progressive lung scarring and remodeling. Although treatments exist that slow disease progression, IPF is irreversible, and there is no cure. Cellular senescence, a major hallmark of aging, has been implicated in IPF pathogenesis, and mitochondrial dysfunction is increasingly recognized as a driver of senescence. Adenine nucleotide translocases (ANTs) are abundant mitochondrial ATP–ADP transporters critical for regulating cell fate and maintaining mitochondrial function. We sought to determine how alterations in ANTs influence cellular senescence in pulmonary fibrosis. We found that *SLC25A4* (solute carrier family 25 member 4) (ANT1) and *SLC25A5* (ANT2) expression is reduced in the lungs of patients with IPF, particularly within alveolar type II (AT2) cells, by single-cell RNA sequencing and tissue staining. Loss of ANT1 by siRNA in lung epithelial cells resulted in increased senescence markers such as β-galactosidase and p21, with a reduction in the ratio of nicotinamide adenine dinucleotide to reduced nicotinamide adenine dinucleotide. Bleomycin-treated ANT1 knockdown cells also had increased senescence markers compared with bleomycin-treated control cells. Loss of ANT1 in AT2 cells resulted in a reduction in alveolar organoid growth, with an increase in p21 by staining. Global loss of ANT1 resulted in worse lung fibrosis and increased senescence in the bleomycin- and asbestos-induced mouse models of pulmonary fibrosis. In summary, loss of ANT1 contributes to IPF pathogenesis through mitochondrial dysfunction, increased senescence, and decreased regenerative capacity of AT2 cells, resulting in enhanced lung fibrosis. Modulation of ANTs presents a new therapeutic avenue that may alter cellular senescence pathways and limit pulmonary fibrosis.

Keywords: IPF; adenine nucleotide translocase; senescence; bleomycin; mitochondria

Idiopathic pulmonary fibrosis (IPF) is a deadly and progressive lung disease characterized by irreversible lung scarring (fibrosis), parenchymal and vascular remodeling, and dysregulated epithelial repair (1). Current treatments include antifibrotic agents that have limited efficacy in reversing or preventing the disease (2). Studies have demonstrated that in addition to a loss of alveolar epithelial cells in the IPF lung (3), complex changes occur in the remaining lung epithelial cells. These alveolar epithelial cells undergo functional reprogramming and acquire "transitional" cell states not typically seen in the healthy lung (3, 4). A deeper understanding of the mechanisms that result in epithelial cell loss and abnormal alveolar repair is needed to develop targeted therapeutics that can stop or even reverse disease progression.

One important component of IPF pathogenesis is cellular senescence (5), a permanent state of cell-cycle arrest that plays a role in several aging-related diseases (6, 7).

(Received in original form August 11, 2022; accepted in final form July 24, 2023)

*Co–first authors.

Supported by National Heart, Lung, and Blood Institute/National Institutes of Health grants T32 HL007563 (J.C.B.), F30HL165827 (J. Sui), R01HL141380 (M.K.), U54AG075931 (M.K.), and 5K08-HL141595 (C.R.K.); the Burroughs Wellcome Fund Career Award for Medical Scientists (C.R.K.); and the Parker Foundation Parker B. Francis Fellowship (C.R.K.).

Author Contributions: Conceived the experiments: C.R.K., J. Sui, and J.C.B. Collection of samples: J.C.B., J. Sui, J. Shi, and C.R.K. Performed the experiments: C.R.K., J.C.B., J. Sui, J. Shi, Q.H., and X.L. Data analysis: C.R.K., J. Sui, J.C.B., and Q.H. Wrote the paper and figure creation: J. Sui, J.C.B., and C.R.K. Critical review and approval: Y.Z., M.K., and C.R.K. All authors reviewed the manuscript and approved the final version prior to submission.

Correspondence and requests for reprints should be addressed to Corrine R. Kliment, M.D., Ph.D., Pulmonary Allergy and Critical Care Medicine, Department of Medicine, University of Pittsburgh, W1254, Biomedical Science Tower, 200 Lothrop Street, Pittsburgh, PA 15213. E-mail: ckliment@pitt.edu.

This article has a related editorial.

This article has a data supplement, which is accessible from this issue's table of contents at www.atsjournals.org.

Am J Respir Cell Mol Biol Vol 69, Iss 5, pp 556–569, November 2023

Originally Published in Press as DOI: 10.1165/rcmb.2022-0315OC on July 24, 2023
Internet address: www.atsjournals.org

Clinical Relevance

This study advances our knowledge of how mitochondrial dysfunction contributes to cellular senescence, epithelial regenerative capacity, and the pathogenesis of pulmonary fibrosis.

Senescent cells are metabolically active cells that often resist apoptosis and accumulate in organs as part of an aging-associated stress response to stimuli. Mitochondrial dysfunction has been increasingly recognized as an important inducer of senescence (8), but additional research is necessary to define this process. Changes in mitochondrial structure and function have been implicated in aging and IPF and have been observed primarily in lung epithelial cells, fibroblasts, and macrophages (9–11). Mitochondrial dysfunction and senescence have recently been described in IPF (8, 12, 13). The cellular factors driving mitochondrial-induced senescence and lung fibrosis progression remain unclear and warrant more investigation.

The gene expression profile of senescent cells is characteristically altered compared with nonsenescent cells (14), most notably with upregulation of cell-cycle inhibitors such as $p16^{INK4a}$ and $p21^{CIP1/WAF1}$, tumor suppressor protein p53, and increased lysosomal β-galactosidase (β-gal) activity. Senescent cells also secrete a milieu of signaling molecules, including proinflammatory chemokines and growth factors, collectively known as the senescence-associated secretory phenotype (SASP) (15), that may propagate inflammation and tissue remodeling. Upregulation of these senescence markers and SASP have been identified in epithelial cells and fibroblasts in lung fibrosis (5, 16). The clearance of these senescent cells and SASP inhibition have both been found to enhance pulmonary function in mouse models (17, 18). Thus, the identification of pharmacological treatments that target senescent cells or SASP suppression might be promising avenues of IPF treatment.

Adenine nucleotide translocases (ANTs; human paralogs ANT1–4) are mitochondrial ATP-ADP transporters that are critical for mitochondrial bioenergetics, reactive oxygen species production, and regulation of cell fate (19, 20). ANT1 and ANT2 are expressed in the human lung (21). Several mutations in ANTs, particularly in ANT1, have been described in human mitochondrial disease (22). Null and point mutations of ANT1 result in mitochondrial myopathy, hypertrophic cardiomyopathy, lactic acidosis, and ophthalmoplegia (22). Despite evidence that ANT1 is important for maintaining mitochondrial function, the role of ANT1 in cellular senescence and lung disease has not yet been described. By leveraging human lung tissue and the bleomycin and asbestos injury models in mice, we sought to determine how alterations in ANT1 influence cellular senescence in pulmonary fibrosis.

Methods

See the data supplement for expanded methods.

Human Lung Tissue Studies

Human lung tissue samples were obtained from the Tissue Core at the University of Pittsburgh (supported by National Institute of Diabetes and Digestive and Kidney Diseases grant P30 DK072506 and the Cystic Fibrosis Foundation's Research Development Program). Control lung samples originated from lungs deemed unsuitable for organ transplantation. All IPF lungs were explanted from patients with IPF undergoing lung transplantation (STUDY18100070). Genomic data were obtained from the Lung Genomics Research Consortium (LGRC) (Gene Expression Omnibus: GSE47460) (23) using tissue samples and clinical data collected through the Lung Tissue Research Consortium. Single-cell RNA sequencing (scRNA-seq) data are publicly available (Gene Expression Omnibus: GSE190889), Bulk RNA sequencing data is accessible through Gene Expression Omnibus GSE244305, along with a GitHub repository (https://github.com/KonigshoffLab/GPR87_IPF_2022) (24). *See* the data supplement.

Bleomycin and Asbestos Mouse Models

All animal studies were approved by the University of Pittsburgh Institutional Animal Care and Use Committee. ANT1-null mice were a gift from Douglas Wallace (University of Pennsylvania). Male and female mice (10–12 wk old, $n = 6$–10 per group) were treated with intratracheal bleomycin sulfate (0.05 U per 25 g mouse with dose adjustments for weight), saline control, crocidolite asbestos, or titanium dioxide (an inert control particle) (0.1 mg in saline) (25). Mice were killed at 28 days after treatment. BAL was collected, and lungs were inflated with 10% formalin at 25 cm^2 H_2O and formalin fixed for 24 hours before paraffin embedding or flash frozen for protein analysis, RNA isolation, and hydroxyproline quantification. BAL cytokine concentrations were measured using a Luminex Cytokine Multiplex Panel (R&D Systems).

Immunocytochemistry of Mouse and Human Lung Tissue

Immunofluorescent staining of lung tissue was completed as previously described (21). Lungs from patients with IPF and normal control lungs were formalin fixed and paraffin embedded. Human and mouse lung sections were stained for ANT1 (catalog #ab102032; Abcam), ANT2 (catalog #192410; Abcam), HTII-280 (catalog #TB-27AHT2-280; Terrace Biotech), ABCA3 (ATP binding cassette subfamily A member 3) (catalog #WRAB-70565; Seven Hills Bioreagents), and secondary Alexa fluorophore antibodies (Molecular Probes). Control sections were stained with nonimmune rabbit IgG (catalog #2729P; Cell Signaling Technology). Mouse primary alveolar organoids were stained using rat anti-p21 and ABCA3 antibodies. Images were acquired using a Nikon A1R confocal microscope.

Cell Culture and Targeted Gene Suppression

Human bronchial epithelial cell lines include HBEC3-KT (American Type Culture Collection [ATCC]), BEAS-2B (ATCC), and alveolar epithelial A549s (ATCC). Cells were transfected with 150 nM siRNA ON-TARGETplus SMARTpools (Dharmacon: ANT1 [*SLC25A4* (solute carrier family 25 member 4), catalog #L-007485-00-0005], ANT2 [*SLC25A5*, catalog #L-007486-02-0005], and nontargeting control pool [catalog #D-001810-10-05]) using Lipofectamine 3000 (Invitrogen) per the manufacturer's protocol. CRISPR knockout (KO) clones were generated for *SLC25A4* (ANT1). To induce senescence, Beas-2B and A549 cells were treated with 10 mg/ml bleomycin over 2 days. Bulk RNA sequencing, real-time quantitative PCR (qPCR), Seahorse metabolic tests (Agilent), nicotinamide adenine dinucleotide (NAD^+):reduced NAD^+ (NADH) and ATP assays, western blot, and β-gal staining

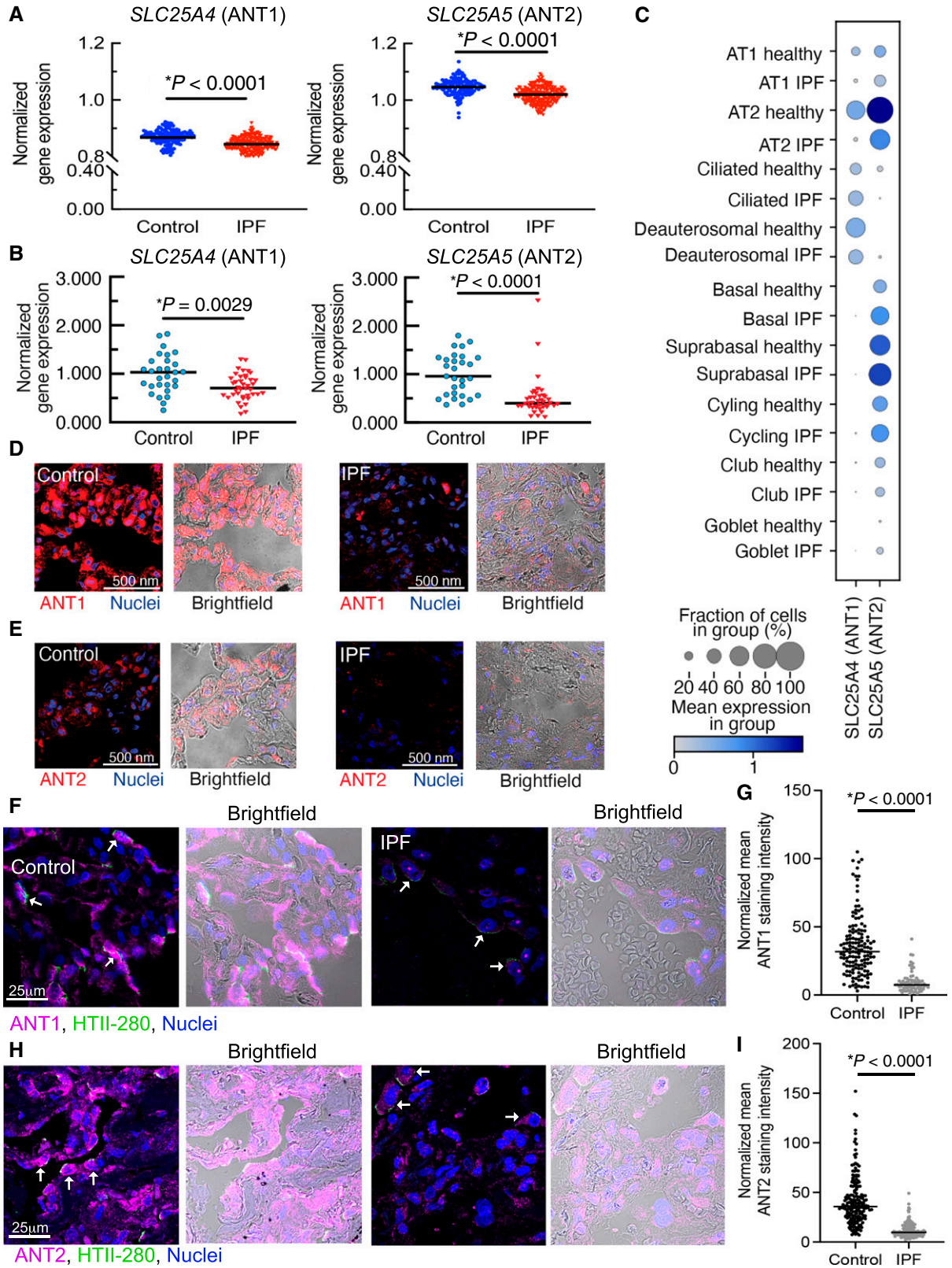

Figure 1. *SLC25A4* (solute carrier family 25 member 4) (ANT1 [adenine nucleotide translocase 1]) and *SLC25A5* (ANT2) expression is decreased in alveolar type II (AT2) cells in the lungs of patients with idiopathic pulmonary fibrosis (IPF). (*A*) A human microarray data set shows that gene expression of *SLC25A4* (*$P < 0.0001$) and *SLC25A5* (*$P < 0.0001$) is significantly decreased in whole-lung lysates from patients with IPF ($n = 255$) compared with healthy control subjects ($n = 137$) (Lung Genomics Research Consortium; 1RC2HL101715). Genomic data are

were completed. *See* the data supplement for details.

Primary Mouse Alveolar Organoids

Primary alveolar type II (AT2) cells were isolated from mouse lungs (wild-type [WT] and Ant1 KO) as previously published (26) using $CD45^+$/$CD31^+$–negative selection and epithelial cell adhesion molecule–positive selection. Cells were cocultured in Matrigel (Corning) with mouse fibroblasts. Growth was monitored over 14 days using a BioTek Cytation imager (Agilent).

Statistics

Mean densitometry (Image Lab software; Bio-Rad) and all other quantitative data (mean ± SEM) are normalized to appropriate control groups. Statistical analyses were completed using GraphPad Prism 9.3. Data are assessed for sample distribution. If samples are normally distributed, then data are analyzed using ANOVA with the Fisher least significant difference *post hoc* test. If the data are not normally distributed, nonparametric analyses, including Kruskal-Wallis, Tukey, and/or Mann-Whitney, are used.

Results

ANT Expression Is Reduced in the Lungs of Patients with IPF

To determine whether ANTs play a role in IPF pathogenesis, we compared whole-lung tissue gene expression for *SLC25A4* (ANT1) and *SLC25A5* (ANT2) in lung tissue from patients with IPF (Figure 1A) using an Illumina microarray data set from the LGRC. We found that gene expression for *SLC25A4* ($P < 0.0001$) and *SLC25A5* ($P < 0.0001$) was significantly reduced in the lungs of patients with IPF ($n = 255$) compared with healthy control subjects ($n = 137$) (Figure 1A). To validate these findings, we confirmed that *SLC25A4* and *SLC25A5* mRNA concentrations are reduced in the lung tissue of patients with IPF from a separate cohort of IPF ($n = 40$) and normal control ($n = 29$) lung by real-time qPCR (Figure 1B; $P = 0.0029$ for *SLC25A4* and $P < 0.0001$ for *SLC25A5*). We next used a human scRNA-seq data set of epithelial cell adhesion molecule–positive lung epithelial cells isolated from healthy control and IPF lungs to obtain a more comprehensive understanding of how *SCL25A4* and *SLC25A5* transcript levels change among different epithelial cell types. Gene expression of *SCL25A4* and *SLC25A5* was markedly reduced in alveolar type I (AT1) and AT2 cells (specifically identified using *SFTPC* and *SFTPB* [surfactant protein B] expression) from IPF lungs compared with normal lungs (Figure 1C). To further localize the expression of ANT proteins in the lung *in situ*, we stained human lung sections from three patients with IPF and three healthy control subjects for ANT1 and ANT2 proteins (Figures 1D and 1E; *see* Figure E1 in the data supplement). Importantly, we found that ANT1 and ANT2 protein expression was moderately reduced in alveolar cells in fibrotic alveolar tissue from the IPF group compared with the alveolar tissue from the control subjects. AT2 cells are a key regenerative cell type that are affected in IPF, and the scRNA-seq data show notable reductions in *SLC25A4* and *SLC25A5* in AT2 cells. Therefore, we next used immunofluorescence colocalization, which demonstrated that both ANT1 (Figures 1F and 1G) and ANT2 (Figures 1H and 1I) are significantly reduced in AT2 cells (HTII-280–positive cells, shown in green). Together, these observations show that ANT1 and ANT2 expression is reduced in fibrotic lung tissue at the RNA and protein levels, particularly in AT2 cells. This supports the notion that the loss of ANTs may play an important role in alveolar epithelial cell function and might contribute to the pathogenesis of IPF.

Loss of ANT1 Is Associated with Cellular Senescence

Cellular senescence is associated with proaging stressors and is increasingly implicated as a key mechanism in IPF pathogenesis (5). The cyclin-dependent kinase inhibitors $p16^{Ink4a}$, $p21^{Cip1/Waf1}$, and p53 and positive β-gal staining are established markers of senescence (27, 28). This notion that senescence is associated with IPF pathogenesis is supported in our LGRC whole-lung tissue gene expression, which shows significant upregulation in *CDKN2A* (cyclin dependent kinase inhibitor 2A) (p16; $P < 0.0001$) and *TP53* (tumor protein P53) (p53; $P < 0.0001$) gene expression in the lung tissue of the IPF cohort (Figure 2A). Interestingly, we found that *CDKN2A* expression is inversely correlated to *SLC25A4* (ANT1) ($P < 0.0001$) and *SLC25A5* (ANT2) ($P < 0.0001$) expression in the IPF cohort (Figure 2B), as well as in our scRNA-seq data set from isolated lung epithelial cells from IPF lung tissue. Both *SLC25A4* (ANT1) and *SLC25A5* (ANT2) gene expression were inversely correlated to a number of common cellular senescence genes when analyzing all epithelial cells (Figure 2C), specifically AT1 and AT2 cells (Figure 2D). Gene expression correlation tables are provided in Tables E1 and E2. Together these data show that gene expression of *SLC25A4* (ANT1) and *SLC25A5* (ANT2) are reduced in alveolar epithelial cells in IPF and may influence cellular senescence in IPF.

Figure 1. (*Continued*). normalized to glucose-6-phosphate isomerase. Statistics are calculated using Student's *t* test with the Mann-Whitney *post hoc* test. Median bars are shown. (*B*) Real-time quantitative PCR shows significant decreases in *SLC25A4* (**P* = 0.0029) and *SLC25A5* (**P* < 0.0001) gene expression in lung homogenates from a separate cohort of patients with IPF ($n = 40$) compared with healthy control lungs ($n = 29$). Statistics are calculated using the unpaired nonparametric Mann-Whitney test. (*C*) Single-cell RNA sequencing results obtained on isolated lung epithelial cells from patients with IPF and normal control subjects. Mean expression and fraction of cells with gene expression of *SLC25*A4 and *SLC25A5* for each cell cluster type are depicted. (*D* and *E*) Representative immunofluorescence staining for (*D*) ANT1 (catalog #ab102032 [Abcam] rabbit polyclonal, 1:500) and (*E*) ANT2 (catalog #192410 [Abcam] rabbit polyclonal, 1:100) in human lung tissue sections from healthy control subjects and patients with IPF. Images from additional patient samples are available in Figure E1 ($n = 4$ subjects per group). Scale bars, 500 nm. (*F–I*) Representative immunofluorescence costaining and quantification for HTII-280 (AT2 cell marker) and ANT1 (*F* and *G*) (catalog #ab102032; Abcam) and ANT2. (*H* and *I*) (catalog #192410; Abcam) in lung tissue from healthy control subjects and patients with IPF. The white arrows indicate representative AT2 cells. ANT staining intensity was quantified in HTII-280^+ cells across images (six to nine images per patient, $n = 2$ patients per group). Statistics are calculated using the unpaired nonparametric Mann-Whitney test. Scale bars, 25 μm. **P* value < 0.0001. All images were obtained using confocal microscopy at 60×. Brightfield overlay images and scale bars are provided. AT1 = alveolar type I.

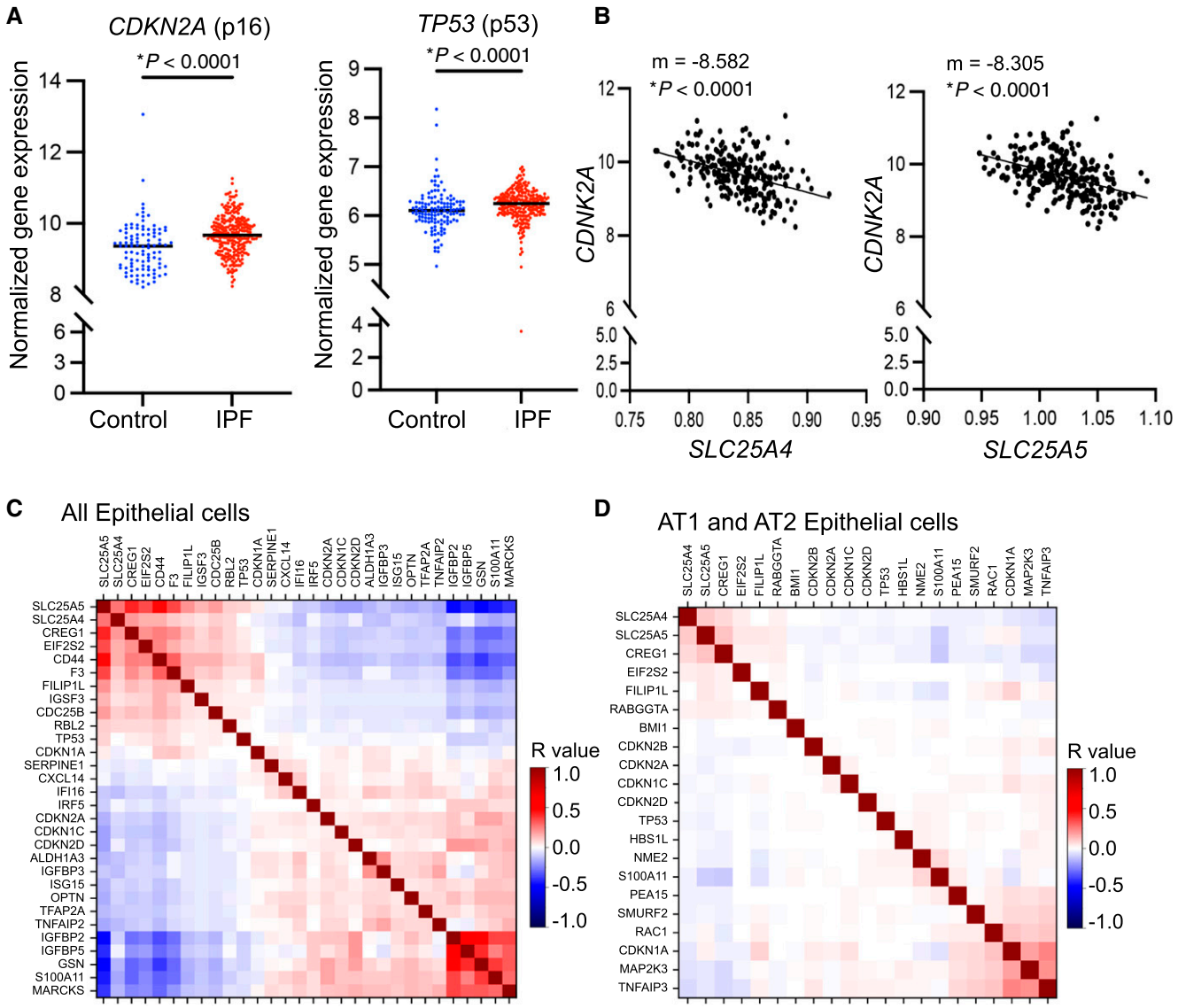

Figure 2. ANT gene expression inversely correlates with markers of cellular senescence. (*A*) Gene expression data from the Lung Genomics Research Consortium microarray data set shows that *CDKN2A* (cyclin dependent kinase inhibitor 2A) (p16) (*$P < 0.0001$) and *TP53* (p53) are significantly increased in whole-lung lysates from patients with IPF ($n = 255$) compared with lysates from healthy control subjects ($n = 137$). Statistics are calculated using Student's *t* test. *P* values are shown. (*B*) Gene expression correlations between *CDKN2A* and *SLC25A4* (ANT1) (*$P < 0.0001$) and *CDKN2A* and *SLC25A5* (ANT2) (*$P < 0.0001$). Data are normalized to glucose-6-phosphate isomerase. Statistics are calculated using Mann-Whitney unpaired nonparametric tests. Median bars are shown. (*C* and *D*) Gene expression correlations were determined in the human lung epithelial single-cell RNA sequencing data set for *SLC25A4* (ANT1), *SLC25A5* (ANT2), and common genes in the cellular senescence pathway for (*C*) all epithelial cells or (*D*) AT1 and AT2 epithelial cells. Color bar shows the calculated *R* value for each correlation.

To assess if loss of ANT1 expression influences the development of cellular senescence, we used siRNA to suppress ANT1 expression in three immortalized human lung epithelial cell lines, then probed for markers of cellular senescence. Gene knockdown (KD) was confirmed using real-time qPCR (*see* Figure E2A) and has been previously detailed (21). In BEAS-2B cells, ANT1 KD was associated with significant increases in p21 ($P = 0.022$) and p53 ($P = 0.020$) by western blot (Figure 3A). In the HBEC3-KT cell line, ANT1 KD resulted in a significant increase in p21 at baseline and a further increase in p21 after bleomycin treatment, which induces senescence, compared with control siRNA cells (Figure 3B). There was a trend toward an increase in p16 ($P = 0.0817$) with ANT1 KD. In addition, significantly more HBEC3-KT cells were stained positive for senescence-associated β-gal and increased cell-body size with ANT1 KD compared with control cells (Figure 3C), with similar β-gal increases after bleomycin in both groups. Expression for p21 was also significantly increased in the alveolar epithelial cell line A549 with

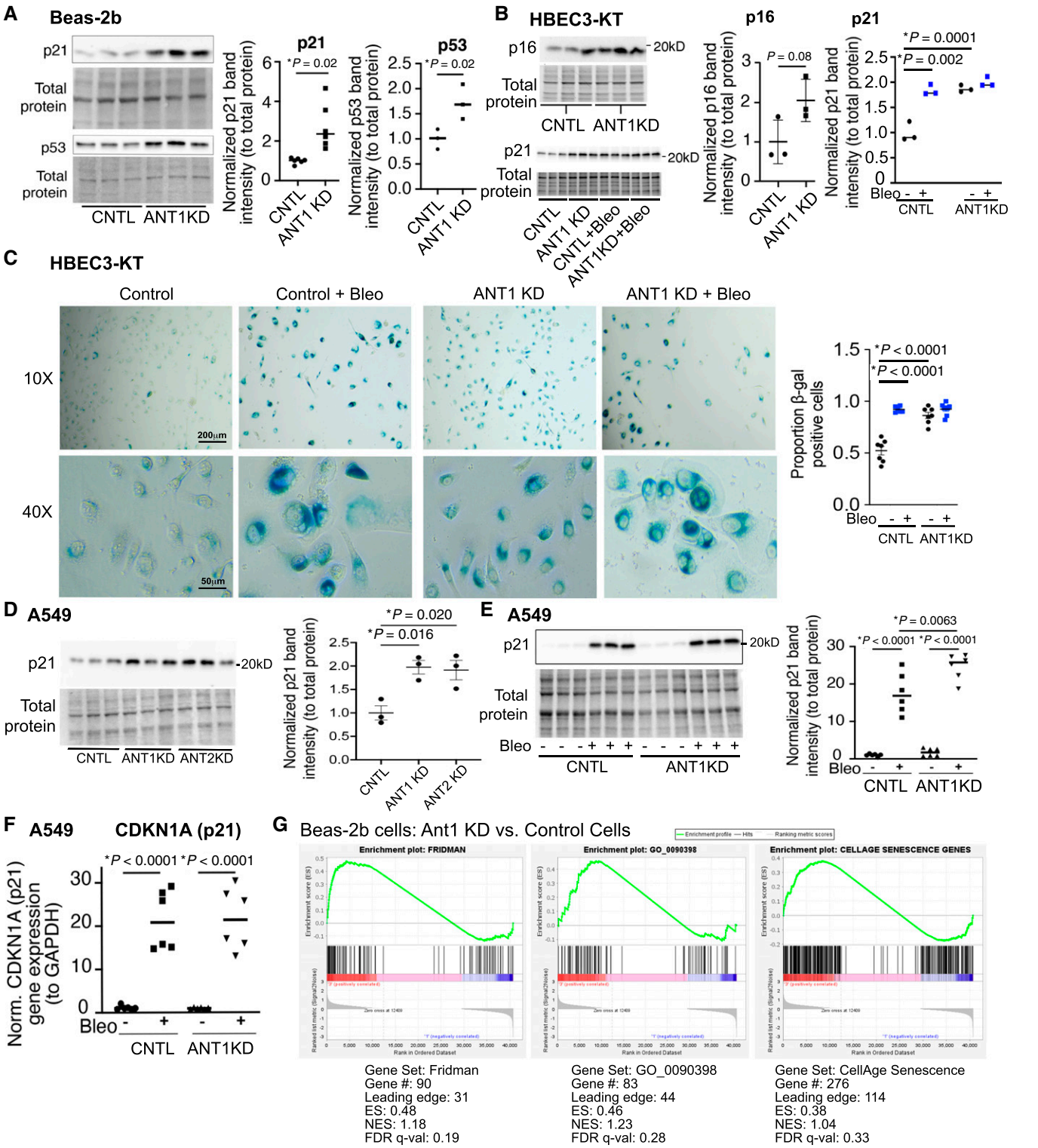

Figure 3. Loss of ANT1 results in increased markers of cellular senescence in multiple lung epithelial cell types. ANT1 expression was knocked down using siRNA compared with scrambled siRNA control (CNTL) conditions. For select experiments, cells were treated with media or bleomycin (Bleo) for 48 hours. *P* values are noted in the figures. (*A*) Western blot and quantification are shown from human bronchial epithelial BEAS-2B cell lysates for p21 (*$P = 0.0220$; $n = 6$) and p53 (*$P = 0.0205$; $n = 3$). (*B*) Western blot analysis was completed on human bronchial epithelial HBEC3-KT cells. Lysates show trending but insignificant increases in p16 ($P = 0.0817$; $n = 3$) and a significant increase in p21 with ANT1 knockdown (KD). Bleomycin treatment led to a further increase in p21. (*C*) Increased senescence-associated β-gal staining (blue) in HBEC3-KT cells with ANT1 KD compared with scrambled siRNA CNTL cells, with increased staining in both groups after bleomycin treatment.

ANT1 KD at baseline (Figure 3D). A further significant increase in p21 induction after bleomycin treatment compared with control siRNA cells (Figure 3E) was also observed. Similar trends were observed at the mRNA level; p21 was significantly increased in both the control ($P < 0.0001$) and ANT1 KD ($P < 0.0001$) groups with bleomycin treatment (Figure 3F). To further confirm our findings of increased senescence with loss of ANT1, we performed bulk RNA sequencing on BEAS-2B cells with ANT1 KD compared with control cells. We performed gene set enrichment analysis demonstrating enrichment of three different senescence gene lists (Fridman, GO_0090398, and CellAge Senescence; *see* Table E3) in cells with ANT1 KD, with the strongest enrichment in the Gene Ontology list (Figure 3G). These observations indicate that loss of ANT1 leads to increased cellular senescence at baseline and increased vulnerability to senescence stimuli in lung epithelial cells.

Loss of ANT1 Is Associated with Altered Metabolic State

To define the mechanism driving cellular senescence with loss of ANT1, we performed metabolic analysis on cells with loss of ANT1. It is well known that mitochondria readily use NAD^+ for many energetic processes (29) and that mitochondrial dysfunction can decrease the NAD^+/NADH redox balance and contribute to senescence. To differentiate between the transient outcomes of ANT1 loss and its long-term effects, we used siRNA for transient ANT1 KD and generated ANT1 CRISPR KO clones in BEAS-2B cells (for KO confirmation, *see* Figure E2C). siRNA KD of ANT1 showed a significant reduction in the normalized NAD^+:NADH ratio (Figure 4A; $P = 0.004$). Similarly, the NAD^+:NADH ratio was significantly reduced in ANT1 KO cells compared with control cells (Figure 4B; $P = 0.015$). ANT1 KD showed a trending but nonsignificant increase in total cellular ATP (Figure 4C), while we observed a statistically significant increase in static level total cellular ATP in ANT1 KOs (Figure 4D; $P = 0.002$). To better understand the effects of ANT1 on real-time mitochondrial energetics, we performed Seahorse analysis using a Mito Stress Test assay. Transient reduction in ANT1 expression with siRNA revealed no significant changes in basal respiration, ATP-linked respiration, or respiration due to proton leak, but the KD of ANT1 conferred a trending but nonsignificant decrease in maximal respiration rate compared with control cells (Figure 4E, upper left panel). On the other hand, the ANT1 KO cells showed a significant increase in basal respiration ($P = 0.0006$), ATP-linked ($P = 0.024$), and maximal ($P < 0.0001$) mitochondrial respiration compared with control cells (Figure 4E, lower left panels). There were also significant increases in basal and maximal extracellular acidification rates in the ANT1 KO cells compared with control cells, suggesting an increase in glycolysis (Figure 4E, lower right panels). This increase in glycolysis would support the increase in total cellular ATP observed in the ANT1 KO cells (Figure 4D). Furthermore, these metabolic changes suggest a compensatory process to preserve energy production in these cells despite an NAD^+/NADH imbalance. Taken together, these data suggest that ANT1 plays a role in maintaining NAD^+/NADH balance and regulating cellular energetics.

Sirtuins are a family of NAD^+-dependent protein deacetylase proteins that have been implicated in senescence and aging. Loss of NAD^+ homeostasis and a reduction in Sirt1 (sirtuin 1) is associated with replicative senescence in human mesenchymal stem cells (30). We found that *Sirt1* gene expression was significantly reduced with bleomycin treatment in ANT1 KD cells (Figure 4F). Furthermore, Sirt1 protein expression was significantly decreased in ANT1 KD cells at baseline and with exposure to bleomycin (Figure 4G). NAD^+:NADH ratio and cellular energy balance are closely linked, so we examined activation of AMPK (AMP-activated protein kinase). Bleomycin treatment led to an increase in total AMPK (Figures 4H and 4I) protein expression in both control and ANT1 KD cells and total ULK (Unc-51 like autophagy activating kinase) in ANT1 KD bleomycin cells (Figures 4H and 4J). There was a trend toward increased phosphorylated AMPK (p-AMPK) with bleomycin treatment in the ANT1 KD cells compared with WT cells (Figures 4H and 4I; p-AMPK, $P = 0.086$; p-AMPK:AMPK ratio, $P = 0.158$), suggesting increased AMPK activation.

These results suggest that loss of ANT1 results in a reduction in NAD^+:NADH ratio at baseline and is also associated with reduced expression of NAD^+-dependent Sirt1 in the context of bleomycin exposure. Both of these processes can promote the senescence phenotype. In summary, our data suggest that loss of ANT1 results in an NAD^+/NADH imbalance and altered metabolic sensing pathways, while cells are able to maintain ATP homeostasis.

Loss of ANT1 Results in Worsened Lung Fibrosis and Inflammation in Mouse Models of Bleomycin and Asbestos Injury

We next used a global Ant1 KO mouse to determine how the loss of Ant1 affects pulmonary fibrosis in the bleomycin and asbestos injury mouse model of pulmonary fibrosis. Gene KD was confirmed in heart, lung, kidney, and liver homogenates using real-time qPCR (*see* Figures E3A and E3B). To model pulmonary fibrosis *in vivo*, mice were treated with bleomycin for 28 days. Notably, Ant1 KO mice treated with bleomycin have increased fibrosis and collagen deposition on hematoxylin and eosin (H&E) (Figure 5A) and trichrome (Figure 5B; for additional full-lung sections, *see* Figure E3C) staining compared with bleomycin-treated control mice. This is

Figure 3. (*Continued*). Scale bars: top panels, 200 μm; bottom panels, 50 μm. (*D*) Western blot was completed on human alveolar A549 cells after ANT1 KD and probed for p21 (*P* values noted). (*E*) ANT1 KD in A549 results in a significant increase in p21 after bleomycin treatment compared with CNTL cells. (*F*) Gene expression for *CDKN1A* (p21) in A549 cells with ANT1 KD (*$P = 0.0063$; $n = 6$). (*G*) Bulk RNA sequencing of BEAS-2B cells with ANT1 KD demonstrates enrichment for senescence genes using gene set enrichment analysis and three separate gene lists. ES, NES, and FDR are noted. All western blot analysis band intensities are normalized to total protein intensity. Data shown are representative of two or three individual experiments. Statistics are calculated using unpaired *t* tests for comparisons between two groups and one-way ANOVA with Kruskal-Wallis tests for comparing more than two groups. Error bars represent SE. β-gal = β-galactosidase; Bleo = Bleomycin; ES = enrichment score; FDR = false discovery rate; NES = normalized enrichment score; Norm. = normalized; q-val = *q* value.

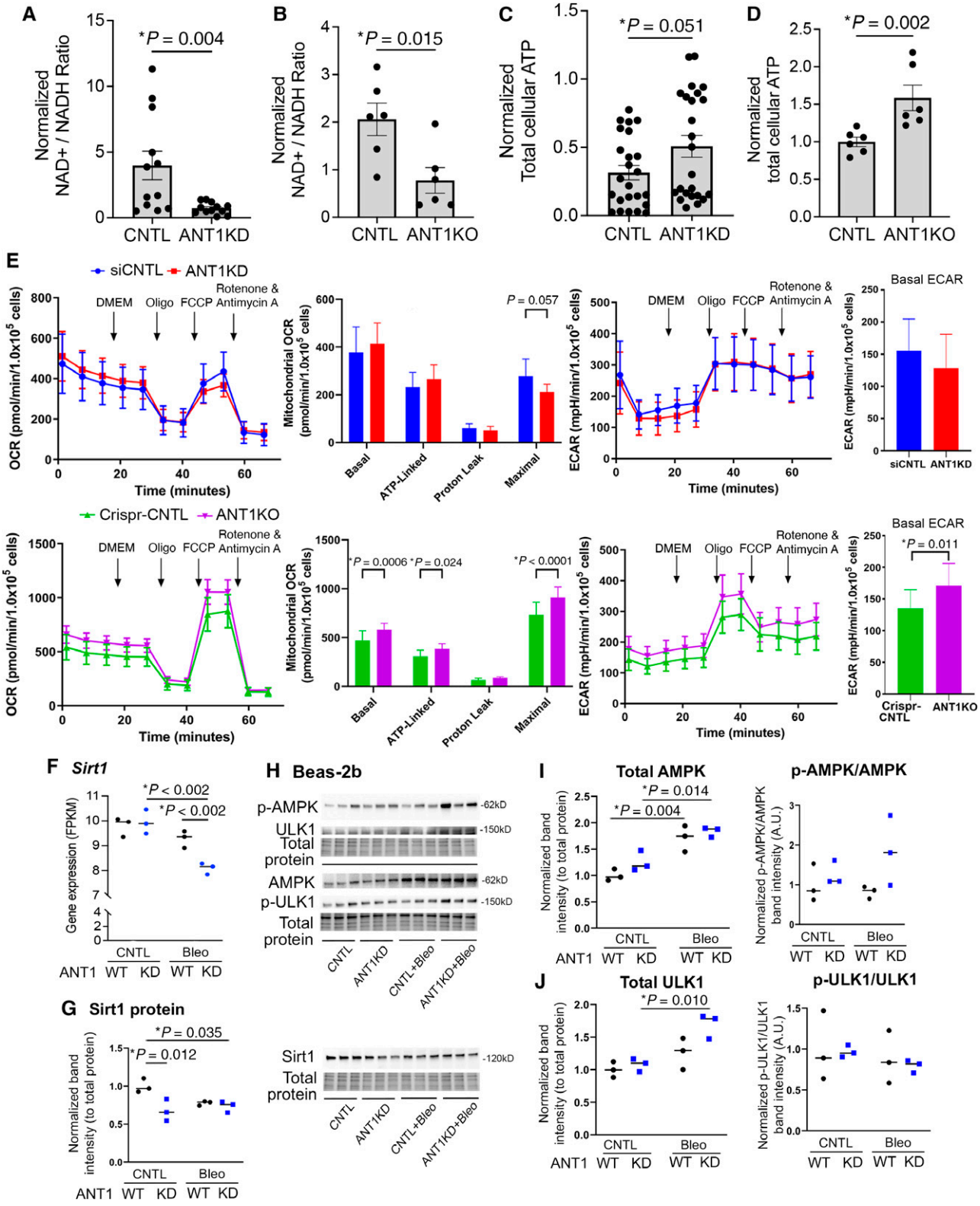

Figure 4. Loss of ANT1 leads to altered nicotinamide adenine dinucleotide (NAD^+)/reduced NAD^+ (NADH) balance and decreased sirt1 (sirtuin 1) expression. In BEAS-2B cells, ANT1 expression was transiently knocked down using siRNA, and ANT1 knockout (KO) clones generated with CRISPR were compared with scramble CNTL. For select experiments, cells were treated with media or bleomycin for 48 hours. (*A* and *B*) Normalized NAD^+:NADH ratios were significantly reduced in cell lysates from (*A*) ANT1 KD (*$P = 0.004$; $n = 12$) and (*B*) ANT1 KO (*$P = 0.015$; $n = 6$) compared with CNTL cells. (*C* and *D*) Normalized total cellular ATP were nonsignificantly increased in cell lysates from (*C*) ANT1 KD

further supported by tissue scoring, with a significant increase in fibrosis index in the bleomycin-treated Ant1 KO mice (Figure 5C; $P = 0.0255$). There was no observed baseline lung phenotype in the Ant1 KO mice treated with saline compared with control mice. We next used intratracheal asbestos exposure as a second model of lung fibrosis. In the asbestos model, Ant1 KO mice treated with asbestos have increased fibrosis on H&E staining (*see* Figure E4A) and increased fibrosis index on tissue scoring (*see* Figure E4B).

Hydroxyproline is a major component of fibrillar collagen, and concentrations are directly correlated to total collagen in tissues. To further support our finding that loss of Ant1 results in increased lung fibrosis, we quantified hydroxyproline on the left lung lobe from the mice to assess collagen content. A significant increase in hydroxyproline concentration was observed in lungs from bleomycin-treated Ant1 KO mice compared with saline-treated control animals (Figure 5D; $P = 0.0088$) and compared with bleomycin-treated WT mice (Figure 5D; $P = 0.0234$). There was a nonsignificant small trend toward increased hydroxyproline in WT mice between the bleomycin- and saline-treated groups.

Cellular senescence is associated with the secretion of a milieu of cytokines, chemokines, growth factors, matrix proteases, and other inflammatory factors, collectively known as the SASP secretome. SASP signaling has been proposed as a mechanism driving inflammation and tissue remodeling in the fibrotic lung (5). To quantify lung tissue inflammation, neutrophil and macrophage infiltration was scored from H&E-stained tissue sections. Bleomycin-induced pulmonary fibrosis was associated with an increase in neutrophil and macrophage indices in both WT and Ant1 KO mice (Figures 5E and 5F). Loss of Ant1 is associated with a significantly greater increase of neutrophils ($P = 0.0035$) and a trending increase in macrophage infiltration ($P = 0.0726$). In the asbestos model, there were no significant differences in neutrophil or macrophage inflammation indices between the WT and Ant1 KO asbestos-treated groups (*see* Figures E4C and E4D). Together, these data demonstrate that loss of Ant1 leads to increased lung fibrosis, collagen deposition, and inflammation in the bleomycin and asbestos lung injury models.

Loss of Ant1 Results in Increased Markers of Senescence and SASP in the Lung

To probe for markers of cellular senescence *in vivo*, we stained mouse lung sections against p21 proteins (Figure 6A). We quantified nuclear amounts of p21 staining within the alveolar regions of the lung tissue using ImageJ (imagej.net) (*see* expanded materials and methods in the data supplement). We found no change in nuclear p21 staining between the saline groups. A significant increase in p21 staining was noted for the bleomycin-treated Ant1 KO mice ($P < 0.0001$) compared with the saline groups and WT bleomycin (Figures 6A and 6B). Staining against p21 was notably higher in the bleomycin Ant1 KO mice compared with the bleomycin-treated WT mice. We localized the increase in p21 to AT2 cells with $ABCA3^{+}$ staining in ANT1 KO lung with and without bleomycin exposure (Figure 6C). AT2 cells serve as stem cells within the lung and are critical for alveolar repair after injury. To determine the effect of loss of ANT1 on AT2 regenerative function, we created alveolar organoids from isolated AT2 cells from WT and ANT1 KO mouse lungs. Loss of ANT1 in AT2 cells resulted in a significant decrease in organoid number (Figure 6D). The size of organoids present was similar between groups. Furthermore, ANT1 KO organoids had increased p21 expression by staining (Figure 6E). These findings suggest that loss of ANT1 contributes to increased AT2 cell senescence and reduced regenerative capacity.

Senescence due to mitochondrial dysfunction has been shown to produce a unique SASP from other senescence stimuli (8), which may be tissue and injury specific. We found that several secreted growth factors and proinflammatory factors associated within the SASP secretome are significantly increased in the BAL from bleomycin-treated Ant1 KO mice, but not WT mice, compared with saline-treated control animals (Figures 7 and E5 and E6 and Table E4). We find that loss of Ant1 is associated with significant enrichment in secreted MMP-12 (matrix metalloproteinase 12; $P < 0.0001$), GDF-15 (growth differentiation factor 15; $P = 0.0139$), and VEGF (vascular endothelial growth factor; $P = 0.0251$) in BAL from bleomycin-treated mice compared with saline-treated control animals. These data support the finding that loss of Ant1 leads to enhanced tissue remodeling in the lung parenchyma after bleomycin treatment. A significant increase in proinflammatory chemokines was also observed in BAL from Ant1 KO mice with bleomycin treatment including CCL3. This chemokine is a key driver of inflammatory cell recruitment, including monocytes and other leukocytes, to the lung environment. There was also an increase in additional proinflammatory markers, including CCL8 ($P = 0.0117$) and GM-CSF (granulocyte–macrophage colony-stimulating factor; $P = 0.0465$) in BAL from bleomycin-treated Ant1 KO mice. Additional factors associated with inflammation are also enriched in BAL from

Figure 4. (*Continued*). (*$P = 0.051$; $n = 24$) and significantly increased in cell lysates from (*D*) ANT1 KO (*$P = 0.002$; $n = 6$) compared with CNTL cells. (*E*) Seahorse Mito Stress Test was performed to measure oxygen consumption rate (OCR) and ECAR on ANT1 KD (upper panel, red/blue; $n = 12$) and ANT1 KO (lower panel, green/purple; $n = 16$) BEAS-2B cells using Seahorse XF96. Cells were sequentially treated with DMEM, Oligo, FCCP, and rotenone/antimycin A. Bar graphs quantify OCRs normalized to cell density, and Student's *t* tests were performed to determine significance. *P* values are noted on the graphs. (*F*) *Sirt1* gene expression was analyzed using bulk RNA sequencing data from BEAS-2B cells with ANT1 KD and treatment with media or bleomycin for 48 hours ($n = 3$). Gene expression is reported as fragments per kilobase per million mapped fragments. All statistics are calculated using two-way ANOVA with Tukey *post hoc* test; *$P < 0.002$. (*G*) Representative western blot for Sirt1 with quantification of normalized band intensity to total protein. *P* values are noted. (*H–J*) Representative western blots for AMPK (AMP-activated protein kinase), ULK1 (Unc-51 like autophagy activating kinase 1), phosphorylated AMPK (p-AMPK), and phosphorylated ULK1 (p-ULK1) with quantification of normalized band intensity to total protein. p-AMPK:AMPK and p-ULK1:ULK1 ratios were calculated and are displayed as a proportion of the CNTL. Statistics for western blots are calculated using two-way ANOVA with Tukey *post hoc* test. **P* values are noted. Data are representative of at least two experiments each. DMEM = Dulbecco's modified Eagle's medium; ECAR = extracellular acidification rate; FCCP = carbonyl cyanide-p-trifluoromethoxyphenylhydrazone; Oligo = oligomycin; WT = wild-type.

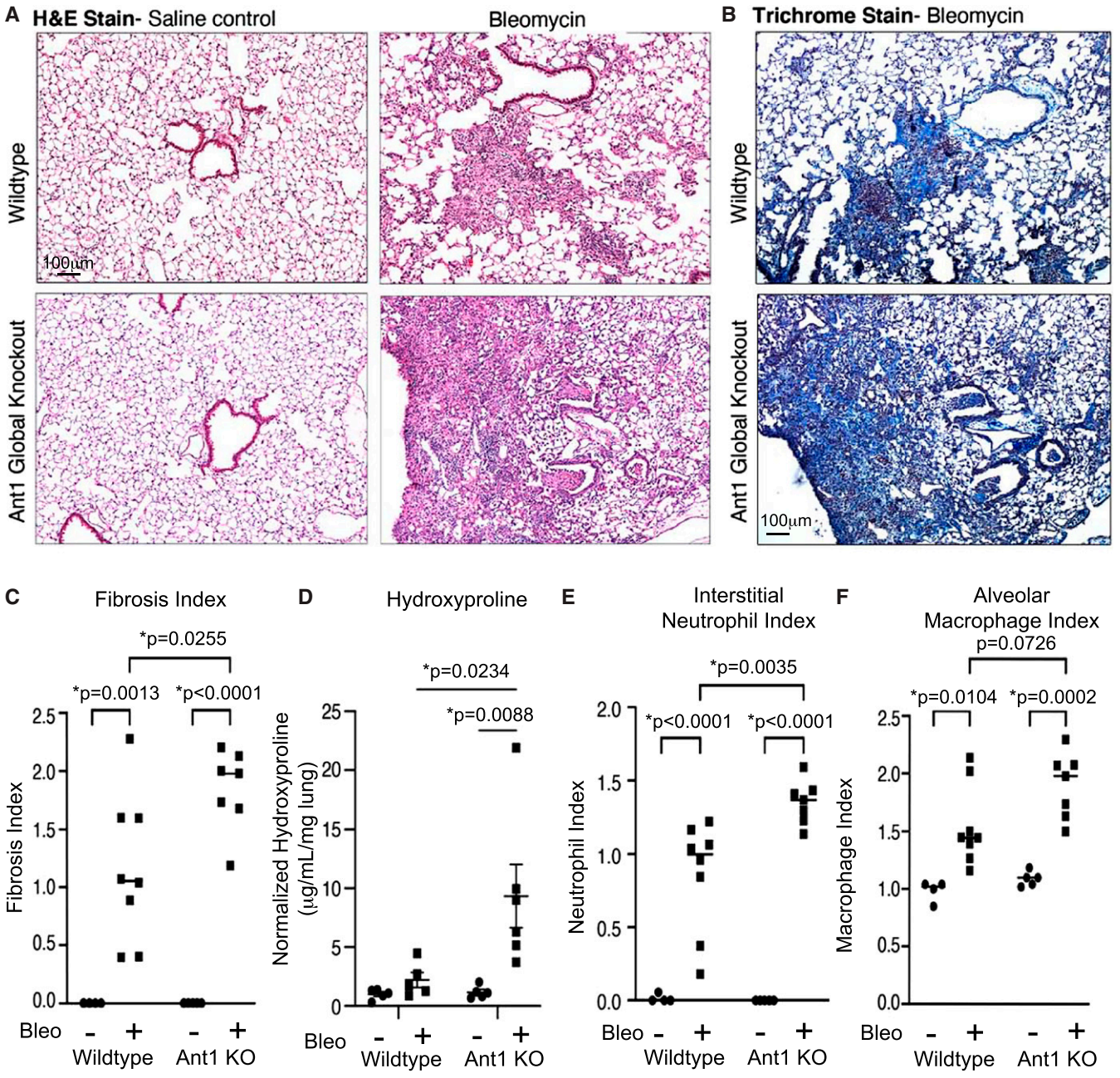

Figure 5. Global KO of ANT1 leads to increased fibrosis and inflammation in murine lungs in a bleomycin model. (*A*) Representative images from H&E staining of paraffin-embedded lung sections from WT and Ant1 KO mice treated with saline or bleomycin for 28 days. Scale bars, 100 μm. (*B*) Representative trichrome stain of paraffin-embedded lung sections from WT and Ant1 KO mice treated with bleomycin for 28 days. Scale bars, 100 μm. (*C*) Tissue scoring fibrosis index for fibrosis quantification. (*D*) Hydroxyproline assay was completed on whole-lung tissue samples (left lung lobe). Number of mouse lungs per group was as follows: WT saline, $n = 5$; WT bleomycin, $n = 5$; Ant1 KO saline, $n = 5$; and Ant1 KO bleomycin, $n = 6$. (*E* and *F*) Tissue scoring indices were determined for (*E*) interstitial neutrophil index and (*F*) alveolar macrophage index. Statistics for all analyses are calculated using ordinary one-way ANOVA with Tukey *post hoc* test. **P* values are noted on the graphs. H&E = hematoxylin and eosin.

bleomycin-treated Ant1 KO mice. Trending but insignificant increases in CXCL1/GROα (growth-regulated oncogene α) ($P = 0.0883$) and IL-7 are also observed in BAL from bleomycin-treated Ant1 KO mice.

A complete list summarizing significant changes in cytokine concentrations is provided in Table E4. These data suggest that loss of Ant1 contributes to the increased proinflammatory response in the lung parenchyma after bleomycin insult by modulating the SASP secretome.

Discussion

Cellular senescence and mitochondrial dysfunction have been implicated in the pathogenesis of IPF, but the factors important for driving senescence related to

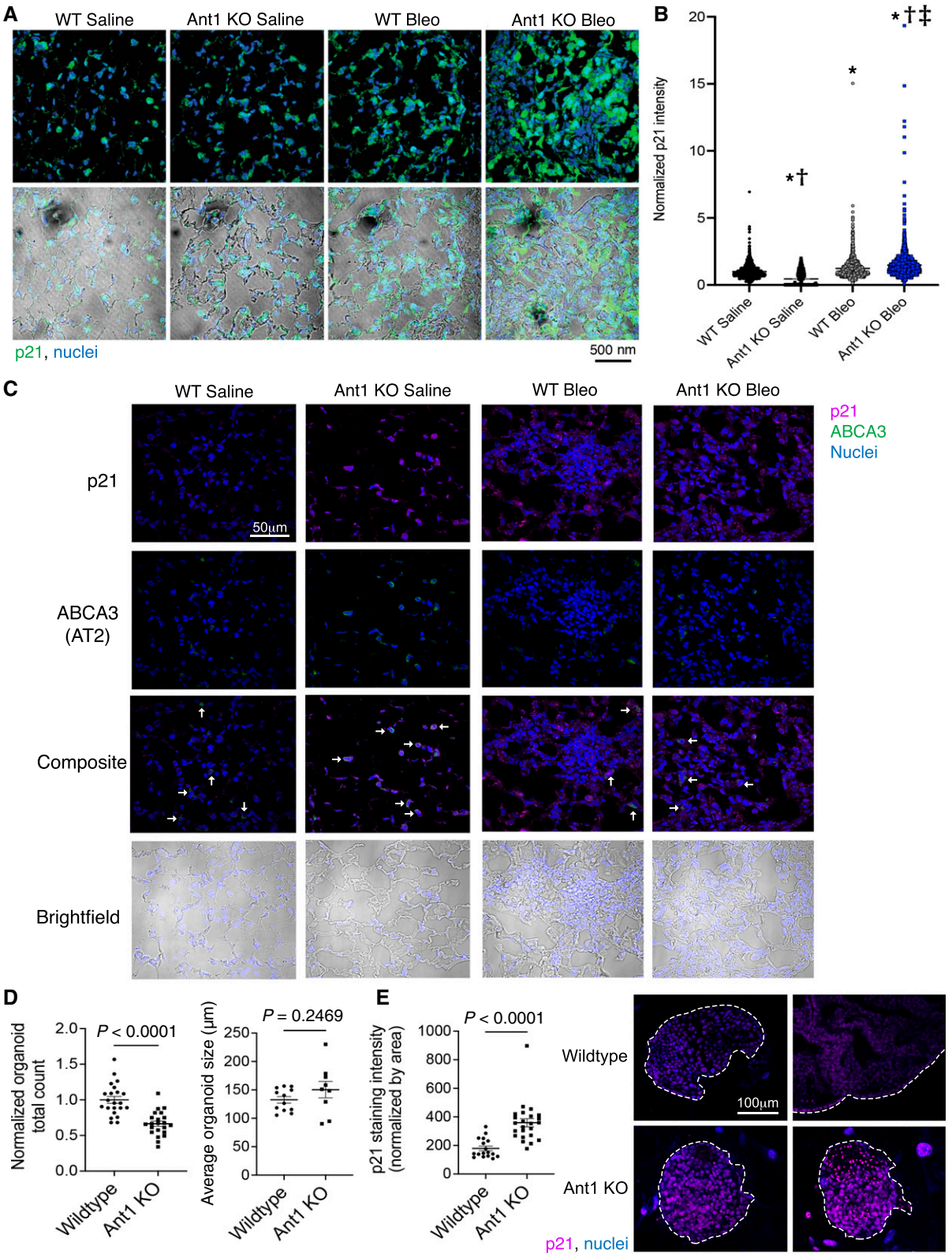

Figure 6. Loss of Ant1 results in increased p21 in pulmonary alveolar tissue after bleomycin injury. WT and Ant1 KO mice were exposed to bleomycin (28 d), and lung tissue was stained for p21 and pro-SFTPC (SPC), a marker of AT2 cells, using immunofluorescence with confocal imaging. (*A*) Representative p21 staining of alveolar lung tissue (green, p21; blue, DAPI-stained nuclei). The bottom row of images shows a brightfield image overlay for lung structure. Scale bars, 500 nm. (*B*) Quantification of nuclear p21 intensity in alveolar tissue areas. Statistics are calculated using

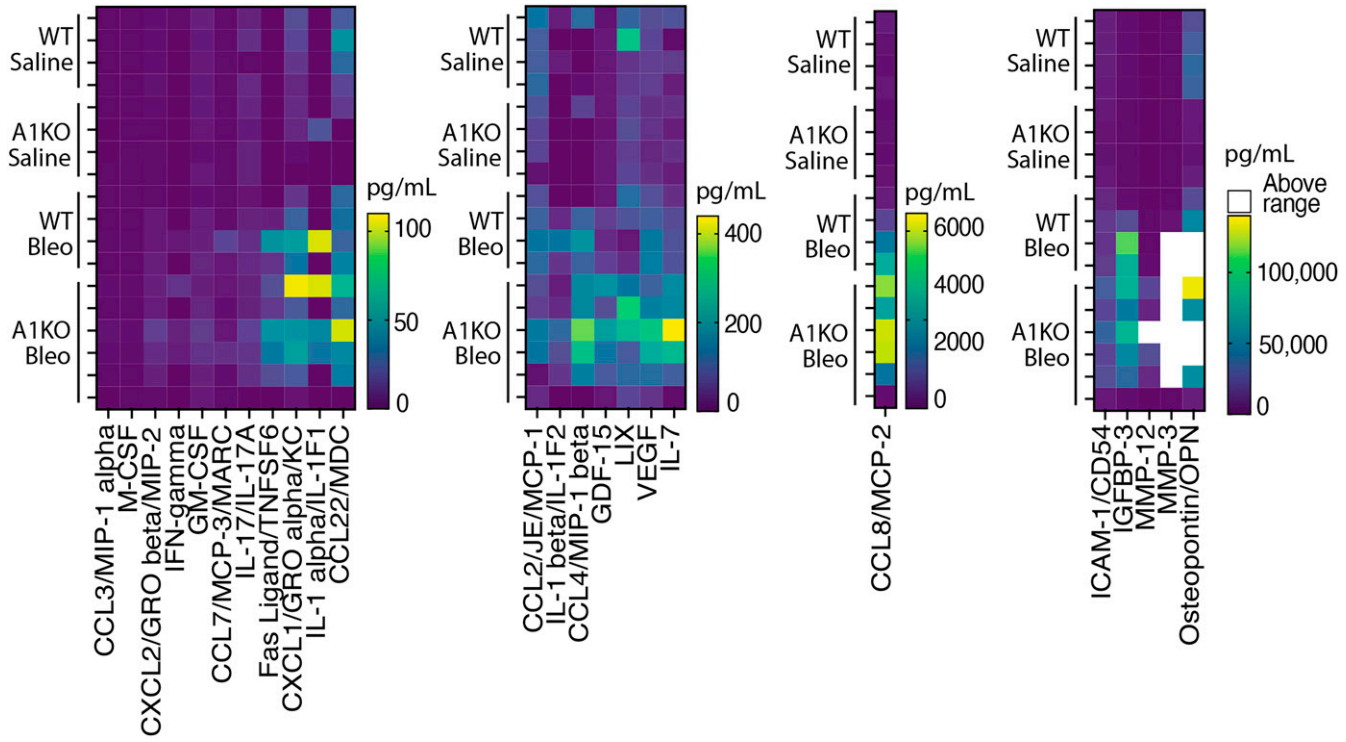

Figure 7. Increased senescence-associated secretory phenotype identified in the BAL with loss of Ant1 and bleomycin injury. Heat maps represent cytokine concentrations in BAL of WT saline ($n = 3$), Ant1 KO saline ($n = 4$), WT bleomycin ($n = 4$), and Ant1 KO bleomycin ($n = 6$) at 28 days after treatment. Cytokine concentrations are shown in picograms per milliliter by color gradients. Select concentrations were above the detection range (white). GDF-15 = growth differentiation factor 15; GM-CSF = granulocyte–macrophage colony-stimulating factor; GRO = growth-regulated oncogene; ICAM-1 = intercellular adhesion molecule 1; MCP-3 = monocyte chemotactic protein 3; M-CSF = macrophage colony-stimulating factor; MDC = macrophage-derived chemokine; MIP-1 = macrophage inflammatory protein 1; MMP = matrix metalloproteinase; OPN = osteopontin; TNFSF6 = Fas ligand; VEGF = vascular endothelial growth factor.

mitochondrial dysfunction remain unclear. The present study is the first to demonstrate that ANT1, a mitochondrial ATP/ADP antiporter, is critical for the regulation of cellular senescence in the lung and IPF by mediating metabolic balance and altering AT2 cell regenerative capacity. Markers of senescence have been identified in epithelial cells within the lungs of patients with IPF (9). In IPF, AT2 alveolar epithelial cells have altered mitochondrial function, represented by a reduction in NAD^+:NADH ratio, reduced ATP, and decreases in the electron transport chain (ETC) complexes (21). Leveraging human IPF lung tissue, we determine that ANT1 and ANT2 are reduced in the AT1 and AT2 lung epithelial cells of patients with IPF, suggesting that depletion of ANTs and subsequent mitochondrial dysfunction or metabolic imbalance are implicated in IPF pathogenesis.

ANTs are abundant ATP/ADP transporters across the inner mitochondrial membrane and are integral to maintaining energy and redox balance in the cell. We have previously demonstrated a direct relationship between loss of ANT1 expression and cellular energetics in lung epithelial cells (21). Mitochondrial dysfunction in IPF has been identified by decreased activity in the ETC, reduced ATP production (31), and increased production of mitochondrial reactive oxygen species (32–34). Mitochondrial dysfunction exacerbates alveolar cell injury and may contribute to fibrogenesis (35, 36). Here, we have shown that loss of ANT1 *in vitro* in cultured human epithelial lung cells and *in vivo* loss of ANT1 results in increased markers of senescence, namely, $p16^{Ink4a}$, $p21^{Cip1/Waf1}$, p53, and positive β-gal. Furthermore, in two mouse models of lung fibrosis, Ant1 deletion resulted in worsened lung fibrosis through enhanced cellular senescence in the lung epithelium. These mice express increased SASP markers in BAL fluid, including chemokines and growth

Figure 6. (*Continued*). one-way ANOVA with Kruskal-Wallis test. $N = 10$–18 images per mouse, with three mice per group. $^*P < 0.0001$ versus WT saline, $^\dagger P < 0.0001$ versus WT bleomycin, and $^\ddagger P < 0.0001$ versus Ant1 KO saline. (*C*) Representative colocalization of p21 and pro-SPC in mouse lung tissue. Primary alveolar organoids were grown using AT2 cells isolated from WT and ANT1 KO mouse lung. Organoids were assessed for number and size at Day 7 and p21 staining at Day 14 of growth. Scale bars, 50 μm. (*D*) Quantification of organoid number and size by area. (*E*) P21 staining of individual organoids normalized to area with representative images provided. Scale bars, 100 μm. Data represent quantification from individual inserts of organoids from two separate experiments. Statistics are calculated using Mann-Whitney Student's *t* test. *P* values are noted. ABCA3 = ATP binding cassette subfamily A member 3.

factors such as GDF-15, a biomarker of epithelial stress upregulated in lungs of patients with IPF (37). This increase in secreted SASP factors likely contributes to the propagation of lung injury seen in the lung with loss of Ant1. These findings highlight the importance of understanding how SASP may change with senescence induced by various etiologies leading to mitochondrial dysfunction. Prior studies of mitochondrial dysfunction–induced senescence used depletion of mitochondrial DNA (8) to induce mitochondrial dysfunction and stress with a unique SASP that lacked IL-1 signaling. In our study, we found an intact IL-1 response but enhanced growth factors and chemokines, suggesting that SASP induced by loss of ANTs in the context of injury differs and requires further investigation.

Loss of ANTs results in a reduction in mitochondrial oxidative respiration (21) due to altered ATP transport out of mitochondria, resulting in a backup of the ETC. Emerging evidence suggests that sensors of the energetic and metabolic state of the cell are important in senescence, specifically NAD^+:NADH ratio and AMPK (8). Oxidized NAD^+ and NADH are important molecules that act as energy sensors within the cell. NAD^+/NADH participate in oxidation–reduction reactions in the tricarboxylic acid cycle, therefore influencing cellular metabolism. NAD^+ is also a key cosubstrate for many cellular processes, including the sirtuin family of proteins (Sirt1 to Sirt7), which are deacylases associated with cellular aging. Replicative senescence in human mesenchymal stem cells has been shown to be associated with loss of NAD^+ homeostasis and a reduction in Sirt1 (30) and can improve cellular life span if enhanced (38). Furthermore, loss of NAD^+/NADH balance and metabolic dysfunction have been found in numerous age-related metabolic disorders of varying organ systems, including pulmonary fibrosis, and recovery of intracellular NAD^+ concentrations has been shown to be protective against lung fibrosis in mouse models (39, 40). Mechanistically, loss of ANT1 appears to drive senescence, with features of the SASP phenotype, by altering the energetic homeostasis in lung epithelial cells, most notably via NAD^+/NADH and sirt1 imbalance. The cellular energetic state in the context of ANT1 deficiency also affects ATP and AMPK signaling and is complex. Overall, the interplay among NAD^+/NADH, ATP metabolism, and ANT1 requires additional investigation.

Our findings suggest that both ANT1 and ANT2 have a role in cell-fate determination in lung epithelial cells, with enriched expression in AT2 cells. ANT2 has greater expression in epithelial cells on the basis of scRNA-seq data in human lung. However, it remains unclear if one isoform plays a larger role specifically in AT2 cell senescence, and if this process is mediated by a different mechanism. This is particularly challenging to dissect in the human lung. Determination of these potential isoform differences requires future isoform-specific studies in the lung. Our prior studies in ciliated cells suggested that ANT2 plays a protective role in ciliated airway epithelial cells compared with ANT1 (21). ANT1 may be a potential therapeutic target for the treatment of patients with IPF to limit fibrosis development. ANTs have been proposed as a possible method of cell-specific targeting of senolytic drugs, as previous studies report that ANT-deficient cells are more susceptible to the cytotoxic effect of the drug MitoTam (41).

Although our studies indicate that global loss of Ant1 in transgenic mice predisposes epithelial cells to become senescent and causes worse fibrosis in mouse fibrosis models, one limitation is that Ant1 is depleted in all cells in this global KO mouse model. Our data in human IPF lung tissue, mouse models of fibrosis, and multiple lung epithelial cell lines support that loss of ANT1 in lung epithelial cells results in the induction of cellular senescence. Additional studies in primary mouse AT2 cell–derived organoids also recapitulated features of the senescence phenotype, including decreased regenerative capacity in the AT2 cells (42, 43). The role of ANT1 in other cell types, such as immune cells and fibroblasts in the lung, remains unclear and requires further investigation to define the potentially broad contribution of ANT1 in lung repair and fibrosis. Future studies could elucidate this using cell-specific alterations of ANT1 expression in the context of lung injury and senescence.

Conclusions

Our findings suggest that ANT1-related mitochondrial dysfunction may be a key driver of senescence in AT2 cells of the lung through metabolic imbalance and present a potential therapeutic target for limiting fibrosis development in IPF. Therapeutic opportunities could involve senolytic agents or modulation of ANT expression to tune metabolic state and function in epithelial cells. The findings of this study underscore the importance of understanding the role of ANT proteins in senescence, AT2 cell function, and lung disease. ■

Author disclosures are available with the text of this article at www.atsjournals.org.

Acknowledgment: The authors thank Mary Jane Duermeyer, Christine Burton, Ian Walsh, Adriana Estrada-Bernal, Yadong Xiao, and Yanwu Zhao for their technical assistance.

References

1. Hutchinson J, Fogarty A, Hubbard R, McKeever T. Global incidence and mortality of idiopathic pulmonary fibrosis: a systematic review. *Eur Respir J* 2015;46:795–806.
2. Wollin L, Wex E, Pautsch A, Schnapp G, Hostettler KE, Stowasser S, *et al.* Mode of action of nintedanib in the treatment of idiopathic pulmonary fibrosis. *Eur Respir J* 2015;45:1434–1445.
3. Yao C, Guan X, Carraro G, Parimon T, Liu X, Huang G, *et al.* Senescence of alveolar type 2 cells drives progressive pulmonary fibrosis. *Am J Respir Crit Care Med* 2021;203:707–717.
4. Adams TS, Schupp JC, Poli S, Ayaub EA, Neumark N, Ahangari F, *et al.* Single-cell RNA-seq reveals ectopic and aberrant lung-resident cell populations in idiopathic pulmonary fibrosis. *Sci Adv* 2020;6:eaba1983.
5. Schafer MJ, White TA, Iijima K, Haak AJ, Ligresti G, Atkinson EJ, *et al.* Cellular senescence mediates fibrotic pulmonary disease. *Nat Commun* 2017;8:14532.
6. Barnes PJ, Baker J, Donnelly LE. Cellular senescence as a mechanism and target in chronic lung diseases. *Am J Respir Crit Care Med* 2019; 200:556–564.
7. Birch J, Barnes PJ, Passos JF. Mitochondria, telomeres and cell senescence: implications for lung ageing and disease. *Pharmacol Ther* 2018;183:34–49.
8. Wiley CD, Velarde MC, Lecot P, Liu S, Sarnoski EA, Freund A, *et al.* Mitochondrial dysfunction induces senescence with a distinct secretory phenotype. *Cell Metab* 2016;23:303–314.
9. Mora AL, Bueno M, Rojas M. Mitochondria in the spotlight of aging and idiopathic pulmonary fibrosis. *J Clin Invest* 2017;127:405–414.

10. Bueno M, Calyeca J, Rojas M, Mora AL. Mitochondria dysfunction and metabolic reprogramming as drivers of idiopathic pulmonary fibrosis. *Redox Biol* 2020;33:101509.
11. Ryter SW, Rosas IO, Owen CA, Martinez FJ, Choi ME, Lee CG, *et al.* Mitochondrial dysfunction as a pathogenic mediator of chronic obstructive pulmonary disease and idiopathic pulmonary fibrosis. *Ann Am Thorac Soc* 2018;15:S266–S272.
12. Wiley CD, Campisi J. The metabolic roots of senescence: mechanisms and opportunities for intervention. *Nat Metab* 2021;3:1290–1301.
13. Schuliga M, Pechkovsky DV, Read J, Waters DW, Blokland KEC, Reid AT, *et al.* Mitochondrial dysfunction contributes to the senescent phenotype of IPF lung fibroblasts. *J Cell Mol Med* 2018;22:5847–5861.
14. Campisi J, d'Adda di Fagagna F. Cellular senescence: when bad things happen to good cells. *Nat Rev Mol Cell Biol* 2007;8:729–740.
15. Coppé J-P, Desprez P-Y, Krtolica A, Campisi J. The senescence-associated secretory phenotype: the dark side of tumor suppression. *Annu Rev Pathol* 2010;5:99–118.
16. Alder JK, Armanios M. Telomere-mediated lung disease. *Physiol Rev* 2022;102:1703–1720.
17. Hashimoto M, Asai A, Kawagishi H, Mikawa R, Iwashita Y, Kanayama K, *et al.* Elimination of $p19^{ARF}$-expressing cells enhances pulmonary function in mice. *JCI Insight* 2016;1:e87732.
18. Calhoun C, Shivshankar P, Saker M, Sloane LB, Livi CB, Sharp ZD, *et al.* Senescent cells contribute to the physiological remodeling of aged lungs. *J Gerontol A Biol Sci Med Sci* 2016;71:153–160.
19. Kretova M, Sabova L, Hodny Z, Bartek J, Kollarovic G, Nelson BD, *et al.* TGF-β/NF1/Smad4-mediated suppression of ANT2 contributes to oxidative stress in cellular senescence. *Cell Signal* 2014;26: 2903–2911.
20. Palmieri F. The mitochondrial transporter family (SLC25): physiological and pathological implications. *Pflugers Arch* 2004;447:689–709.
21. Kliment CR, Nguyen JMK, Kaltreider MJ, Lu Y, Claypool SM, Radder JE, *et al.* Adenine nucleotide translocase regulates airway epithelial metabolism, surface hydration and ciliary function. *J Cell Sci* 2021;134: jcs257162.
22. Stepien G, Torroni A, Chung AB, Hodge JA, Wallace DC. Differential expression of adenine nucleotide translocator isoforms in mammalian tissues and during muscle cell differentiation. *J Biol Chem* 1992;267: 14592–14597.
23. Kusko RL, Brothers JF II, Tedrow J, Pandit K, Huleihel L, Perdomo C, *et al.* Integrated genomics reveals convergent transcriptomic networks underlying chronic obstructive pulmonary disease and idiopathic pulmonary fibrosis. *Am J Respir Crit Care Med* 2016;194: 948–960.
24. Heinzelmann K, Hu Q, Hu Y, Dobrinskikh E, Ansari M, Melo-Narváez MC, *et al.* Single-cell RNA sequencing identifies G-protein coupled receptor 87 as a basal cell marker expressed in distal honeycomb cysts in idiopathic pulmonary fibrosis. *Eur Respir J* 2022;59:2102373.
25. Kliment CR, Englert JM, Gochuico BR, Yu G, Kaminski N, Rosas I, *et al.* Oxidative stress alters syndecan-1 distribution in lungs with pulmonary fibrosis. *J Biol Chem* 2009;284:3537–3545.
26. Lehmann M, Hu Q, Hu Y, Hafner K, Costa R, van den Berg A, *et al.* Chronic WNT/β-catenin signaling induces cellular senescence in lung epithelial cells. *Cell Signal* 2020;70:109588.
27. Lomas NJ, Watts KL, Akram KM, Forsyth NR, Spiteri MA. Idiopathic pulmonary fibrosis: immunohistochemical analysis provides fresh insights into lung tissue remodelling with implications for novel prognostic markers. *Int J Clin Exp Pathol* 2012;5:58–71.
28. Yanai H, Shteinberg A, Porat Z, Budovsky A, Braiman A, Ziesche R, *et al.* Cellular senescence-like features of lung fibroblasts derived from idiopathic pulmonary fibrosis patients. *Aging (Albany NY)* 2015;7: 664–672.
29. Xie N, Zhang L, Gao W, Huang C, Huber PE, Zhou X, *et al.* NAD^+ metabolism: pathophysiologic mechanisms and therapeutic potential. *Signal Transduct Target Ther* 2020;5:227.
30. Yuan X, Liu Y, Bijonowski BM, Tsai A-C, Fu Q, Logan TM, *et al.* NAD^+/NADH redox alterations reconfigure metabolism and rejuvenate senescent human mesenchymal stem cells in vitro. *Commun Biol* 2020;3:774.
31. Zhao YD, Yin L, Archer S, Lu C, Zhao G, Yao Y, *et al.* Metabolic heterogeneity of idiopathic pulmonary fibrosis: a metabolomic study. *BMJ Open Respir Res* 2017;4:e000183.
32. Bueno M, Lai Y-C, Romero Y, Brands J, St Croix CM, Kamga C, *et al.* PINK1 deficiency impairs mitochondrial homeostasis and promotes lung fibrosis. *J Clin Invest* 2015;125:521–538.
33. Jaeger VK, Lebrecht D, Nicholson AG, Wells A, Bhayani H, Gazdhar A, *et al.* Mitochondrial DNA mutations and respiratory chain dysfunction in idiopathic and connective tissue disease-related lung fibrosis. *Sci Rep* 2019;9:5500.
34. Białas AJ, Sitarek P, Miłkowska-Dymanowska J, Piotrowski WJ, Górski P. The role of mitochondria and oxidative/antioxidative imbalance in pathobiology of chronic obstructive pulmonary disease. *Oxid Med Cell Longev* 2016;2016:7808576.
35. Zhou G, Dada LA, Wu M, Kelly A, Trejo H, Zhou Q, *et al.* Hypoxia-induced alveolar epithelial-mesenchymal transition requires mitochondrial ROS and hypoxia-inducible factor 1. *Am J Physiol Lung Cell Mol Physiol* 2009;297:L1120–L1130.
36. Vohwinkel CU, Lecuona E, Sun H, Sommer N, Vadász I, Chandel NS, *et al.* Elevated CO_2 levels cause mitochondrial dysfunction and impair cell proliferation. *J Biol Chem* 2011;286:37067–37076.
37. Zhang Y, Jiang M, Nouraie M, Roth MG, Tabib T, Winters S, *et al.* GDF15 is an epithelial-derived biomarker of idiopathic pulmonary fibrosis. *Am J Physiol Lung Cell Mol Physiol* 2019;317:L510–L521.
38. Ho C, van der Veer E, Akawi O, Pickering JG. SIRT1 markedly extends replicative lifespan if the NAD+ salvage pathway is enhanced. *FEBS Lett* 2009;583:3081–3085.
39. Oh G-S, Lee S-B, Karna A, Kim H-J, Shen A, Pandit A, *et al.* Increased cellular NAD^+ level through NQO1 enzymatic action has protective effects on bleomycin-induced lung fibrosis in mice. *Tuberc Respir Dis (Seoul)* 2016;79:257–266.
40. Liu T, Rinke AE, Wang J, Phan SH. Cellular NAD^+, fibroblast senescence and pulmonary fibrosis. *FASEB J* 2020;34:1.
41. Hubackova S, Davidova E, Rohlenova K, Stursa J, Werner L, Andera L, *et al.* Selective elimination of senescent cells by mitochondrial targeting is regulated by ANT2. *Cell Death Differ* 2019;26:276–290.
42. Lehmann M, Korfei M, Mutze K, Klee S, Skronska-Wasek W, Alsafadi HN, *et al.* Senolytic drugs target alveolar epithelial cell function and attenuate experimental lung fibrosis *ex vivo*. *Eur Respir J* 2017;50:1602367.
43. Hu Y, Ng-Blichfeldt J-P, Ota C, Ciminieri C, Ren W, Hiemstra PS, *et al.* Wnt/β-catenin signaling is critical for regenerative potential of distal lung epithelial progenitor cells in homeostasis and emphysema. *Stem Cells* 2020;38:1467–1478.